GCM clouds and actual clouds as seen from different space lidars : towards a long-term assessment of cloud representation in GCMs using lidar simulators

Marie-Laure Roussel[1], Hélène Chepfer[1], Zacharie Titus[1], and Marine Bonazzola[1]

[1]Laboratoire de Météorologie Dynamique, Palaiseau - France (CNRS)

Correspondence: Marie-Laure Roussel (mlroussel@lmd.ipsl.fr)

Abstract.

In Earth's radiative budget, clouds play a central role but their representation in General Circulation Models (GCMs) remains a major source of uncertainty for climate projection. Here, we used spaceborne lidar observations to assess cloud distribution in the IPSL-CM6-LR model using the CFMIP Observation Simulator Package (COSP). We focused on the lidars onboard CALIPSO and AEOLUS satellites during 2006-2023 and 2018-2023. While CALIPSO has been widely used for GCMs evaluation, AEOLUS was originally designed for wind profiling. However, studies have demonstrated its potential to retrieve reliable cloud profiles. A new module was developed to simulate AEOLUS observations within COSP-lidar, extending original implementations made for CALIPSO, including wavelength change (532nm to 355 nm), viewing geometry (35° off-nadir) and specific parameters adjustments related to sensivity and resolution. We compared our simulations to 1-year observations for both instruments. Results show that AEOLUS observations can effectively evaluate clouds in GCMs, as it shows similar cloud fraction biases in IPSL-CM6-LR to those obtained with CALIPSO. Significant underestimations of low (up to 20%) and high clouds in certain regions (e.g. warm pool) were re-assessed for this model. Sensitivity analyses highlighted the small role of instrument-specific parameters in COSP-lidar: viewing geometry, multiple scattering coefficient and cloud detection threshold (associated with wavelength and sensivity). This work lays the foundation for a consistent multi-decades evaluation of cloud representation using different lidar missions, and supports the integration of EarthCARE/ATLID in COSP-lidar for further model evaluation.

1 Introduction

Clouds play a crucial role in Earth's energy budget by modulating the balance between incoming solar radiation and outgoing thermal radiation. However, cloud feedback processes remain one of the largest sources of uncertainty in climate projections (Boucher et al., 2020), (Bony and Dufresne, 2005), (Vial et al., 2013). Understanding cloud properties and their interactions with radiation is essential for improving climate predictions, as even small changes in cloud characteristics can have significant impacts on global temperature and circulation in the atmosphere (Zelinka et al., 2020; Sherwood et al., 2020). To improve and refine climate models, observational data are indispensable, but measuring clouds precisely at the global scale and capturing their detailed vertical distribution present significant challenges. Spaceborne instruments such as LiDAR (Light Detection And

Ranging, e.g. (Hunt et al., 2009; Wehr et al., 2023)) provide a unique capability to retrieve cloud properties almost everywhere around the globe with high vertical resolution, offering precious insights into cloud properties influencing cloud radiative effects.

However, the validation of cloud representations within Global Climate Models (GCMs) through observational data presents inherent complexities, primarily coming from disparities in model cloud definition and spatial resolution, but also from space-borne instrument configurations. The CFMIP Observation Simulator Package (COSP) (Bodas-Salcedo et al., 2011; Swales et al., 2018) is a tool facilitating direct model to observations comparison by simulating instrument-specific measurements as they would be acquired above the atmosphere modeled by a GCM. By incorporating the capability to simulate measurements from an additional LiDAR in COSP, our goal is to enable comparative studies with models across a broader range of instruments, supporting the on-going evaluation of cloud description and parametrization in CMIP models and multi-model assessments (Cesana and Chepfer, 2013; Cesana et al., 2024; Konsta et al., 2022), and to build a continuous and realistic long-term time-serie of simulations of spaceborne LiDAR observations of clouds from successive spaceborne lidars. Furthermore, these advancements will directly contribute to the final implementation of the EarthCARE lidar (ATLID, (Wehr et al., 2023; Donovan et al., 2024)) module in the COSP algorithm, given its shared instrumental characteristics with AEOLUS (355 nm wavelength, High Spectral Resolution capabilities) (Reverdy et al., 2015; Feofilov et al., 2023).

Extending the COSP-lidar algorithm from previous developments made for CALIOP, the LiDAR of CALIPSO (Chepfer et al., 2008; Guzman et al., 2017; Bonazzola et al., 2023) which was operating from 2008 to 2023, is a key point of this work. We have updated COSP to accurately simulate measurements from different instrumental characteristics than CALIPSO, and especially those of the 355 nm Doppler lidar (ALADIN) onboard AEOLUS from 2018 to 2023. In this study, we used the outputs from the model of the "Laboratoire de Météorologie Dynamique" (LMD) named LMDZ (for its zooming capability), that participates in the CMIP (Climate Model Intercomparison Project) experiments as it is the atmospheric part (Hourdin et al., 2020) of the global model of the IPSL (Institut Pierre-Simon Laplace). In particular, the bias of this model has been extensively evaluated by comparing LMDZ+COSP-lidar/CALIPSO simulations to CALIPSO observations (Cesana et al., 2022). These studies have shown that cloud covers are underestimated in LMDZ with respect to CALIOP measurements, despite the significant improvement of parameterizations from version 5A to 6A (Madeleine et al., 2020). In this context, we conducted COSP-lidar simulations using the LMDZ atmospheric model to compare its cloud representation against observations from two spaceborne lidars: AEOLUS (2020) and CALIPSO (2008). These comparisons aim to assess whether AEOLUS measurements - despite its initial goal of measuring winds and specific instrumental characteristics - can be used like CALIPSO to evaluate the quality of cloud simulations in climate models. Ultimately, our objective is to enable a uniform, long-term, and realistic evaluation framework for cloud representation in models using different spaceborne lidars - CALIPSO, AEOLUS, and now including ATLID on board EarthCARE since 2024.

The paper is organized as follows: Section 2 presents the lidar-based cloud observations from CALIPSO and AEOLUS, and discusses the representativity of the selected years. Section 3 describes the cloud simulations using COSP-lidar, the model

60 used for the inputs (LMDZ), and the analysis of the parameters we modified to simulate AEOLUS-like observations. Section 4 presents the results, including comparisons between AEOLUS and CALIPSO observations, simulations from COSP-lidar driven by LMDZ in CALIPSO and AEOLUS configurations, and their differences with respect to observations. We conclude in Section 5 with a synthesis of the main findings and future perspectives for extending this work toward EarthCARE applications.

2   Cloud observations from space lidars

2.1   Measurements from CALIPSO space lidar

65

The CALIOP (Cloud-Aerosol Lidar with Orthogonal Polarization) instrument on board CALIPSO (Cloud-Aerosol Lidar and Infrared Pathfinder Satellite Observations) satellite is a spaceborne polarization-sensitive lidar operating between 2006 and 2023 designed to provide vertical profiles of clouds and aerosols in the Earth's atmosphere. With its 532 nm and 1064 nm channels, CALIPSO measures backscattered laser signals to derive cloud and aerosol properties, such as optical depth or cloud coverage. CALIPSO operates in a sun-synchronous orbit and crosses the equator at approximately 13:30 local solar time on its ascending node and at 01:30 on its descending node. It operates with a near-nadir viewing geometry, with an inclination of 3° since 2008. After 2018, CALIPSO suffered from major technical issues resulting in a reduced signal strength thus degrading the quality of the measurement dataset (Hunt et al., 2009; Chepfer et al., 2025). This issue was particularly associated with the satellite's passage through the South Atlantic Anomaly (SAA) which is a region over which the onboard electronics can be disrupted by the exposure to high-energy particles (Noel et al., 2014). Here we use the GOCCP v3.14 (GCM-Oriented CALIPSO Cloud Product) dataset, derived from CALIPSO observations (Chepfer et al., 2010; Cesana and Chepfer, 2013). The low energy events have been identified and properly accounted for in this version, ensuring reliable and homogenous quality of the dataset (Chepfer et al., 2025). The cloud detection is done at the higher resolution of the instrument, 75 m cross track and 330 m along track, but here we use the low, mid and high levels cloud covers and cloud fractions profiles at a horizontal resolution of 2° × 2° and vertical resolution of 480 m. Global coverage is provided up to 82° latitude and we choose to use monthly datasets of daily averages, facilitating the evaluation of cloud representation between the observations and the outputs from the climate model.

2.2   Measurements from AEOLUS space lidar

The Atmospheric Laser Doppler Instrument (ALADIN) is a 355 nm High Spectral Resolution (HSRL) spaceborne Doppler Wind LiDAR on board the AEOLUS satellite, primarily designed to retrieve horizontal wind profiles. It also operates in a sun-synchronous orbit and crosses the equator at approximately 18:00 local solar time on its ascending node and at 06:00 on its descending node. It also provides valuable cloud profile observations (Flamant et al., 2008) at a nominal horizontal resolution of 87 km. While it is insufficient for detecting smaller cloud structures, such as shallow cumulus (Feofilov et al., 2022), recent studies have demonstrated that cloud detection is feasible at the full horizontal resolution of 3 km along the orbit track (Wang et al., 2024) of the instrument.

Building on these advances, a similar cloud method has been pursued by Titus et al. (2025) with key modifications compared to Wang et al. (2024). For example, it compensates for the absence of a cross-polar component using a climatology derived from CALIPSO-GOCCP observations and systematically discards hot pixels to enhance detection reliability. For more information about the method, please refer to Titus et al. (2025). Cloud and wind profiles are distributed across different AEOLUS data products at varying spatial resolutions, these datasets have been merged to ensure a fully integrated and usable dataset enabling cloud-wind interactions studies (Titus, 2024).

AEOLUS operates with a laser pointed 35° off-nadir and perpendicular to the satellite track, away from the sun. For consistency with CALIPSO-GOCCP (Chepfer et al., 2010), the reprocessed dataset features a vertical resolution of 480 m and a horizontal resolution of 3 km along the orbit track—the latter matching the highest possible resolution for cloud detection with AEOLUS. The method retrieves cloud fraction profiles at 3 km resolution using AEOLUS Level 1A observations, contributing to improved characterization of cloud structures in spaceborne lidar measurements.

The satellite was launched in 2018 and the mission ended in 2023. In this study, we used the dataset provided by Titus et al. 2025 for the full year 2020.

2.3 Representativity of the selected year

In this study, CALIPSO observations from the year 2008 are primarily used to ensure consistency with the model simulations (see Section 3.1), as the CMIP6 amip forcing data are unavailable for the 2020 year and the AEOLUS cloud product by (Titus, 2024) is only available for 2020. A direct comparison is thus made between CALIPSO measurements and model outputs for 2008 (see Section 4), providing a coherent framework for evaluation. To assess whether such a comparison can be extended to other years, a representativeness analysis is conducted here using CALIPSO data from the 2008–2018 decade, as well as from 2020, a year during which CALIPSO was still in operation but that we won't use for direct comparison to the observations of AEOLUS in 2020 as it is impacted by low power laser shots ((Chepfer et al., 2025)). Also, for a comprehensive analysis of AEOLUS measurements regarding CALIPSO ones we recommend to refer to the study by (Titus, 2024) which, in contrast to the present work, considers the differences in horizontal resolution and in the diurnal cycle captured by the two instruments. As our approach involves comparing datasets from different years, it is essential to assess whether interannual variability in cloud distribution introduces a significant bias. This analysis aims to determine whether the cloud measurements from AEOLUS in 2020 can be meaningfully compared to simulations from 2008, under the assumption that atmospheric conditions remain sufficiently similar. Since CALIPSO and AEOLUS products exhibit highly comparable characteristics, the interannual variability estimated from CALIPSO is assumed to be representative for AEOLUS as well.

To address this issue, we estimate the interannual variability of cloud fraction and cloud cover at high,mid and low levels using the CALIPSO observational time series from 2008 to 2018, which provides a consistent and long-term reference for cloud distribution. The years 2007 and 2016 are excluded from the analysis due to data quality limitations. Specifically in 2007, CALIPSO had not yet adopted its final 3° inclination configuration, while the 2016 year is incomplete in the dataset due to a lack of measurements in February, compromising the reliability of temporal averaging for that year.

	Global mean of yearly means (spatial min/max)		DJF	MAM	JJA	SON
	Median over 10 years	Standard deviation	Median over 10 years	Median over 10 years	Median over 10 years	Median over 10 years
HCC	31% (6,2-82)	4,3% (0,9-13)	31%	31%	31%	30%
MCC	21% (0,7-57)	3,0% (0,2-7,6)	21%	20%	20%	20%
LCC	40% (0-85)	3,5% (0-24)	39%	39%	39%	40%

Table 1. Global mean of yearly and seasonal means of high/mid/low cloud covers for CALIPSO-GOCCP over the 10 years. DJF = December, January, February ; MAM = March, April, May ; JJA = June, July, August ; SON = September, October, November. HCC = High Cloud Cover (P < 440 hPa), MCC = Mid Cloud Cover (440 < P < 680 hPa), LCC = Low Cloud Cover (P > 680 hPa).

125   Figure 1 shows the median (left column) and the standard deviation (right column) of the yearly means (between 2008 and 2018) of respectively high-level (P < 440 hPa), mid-level (440 < P < 680 hPa), and low-level (P > 680 hPa) cloud covers. The median of global mean of high cloud cover is 31%, with a small interannual variability of 4%, but we noticed both very large regional values of high cloud cover - as in the warm pool region where it goes up to 52% - and very little values - as in stratocumulus-dominated areas where it does not exceed 20%. For mid-level cloud cover, the median of global mean is around

130   21%, accompanied by a lower interannual variability of approximately 3%. In contrast, low cloud cover exhibits a median of global mean of 40%, with pronounced spatial variability—ranging from an average of 52% in stratocumulus regions to about 19% over the Indian Ocean.

The mean cloud cover for the years 2008 and 2020 are presented in the figure 3 along with the geographic regions where values deviate significantly from the CALIPSO decadal mean. Areas exceeding three standard deviations from the 10-year

135   average are shaded in gray, indicating that the values are not statistically significant (at the 99.7% confidence level). Based on the assumption of normally distributed, independent, and comparable data, the values respectively observed in 2008 and 2020 that fall within ±3 standard deviations from the 10-year mean indicate no statistically significant deviation from the 2008-2018 decade. The mean cloud cover values for the years 2008 and 2020 at high, middle, and low atmospheric levels are 30%, 20%, and 39% for 2008, and 33%, 22%, and 40% for 2020, respectively. All these values fall within the confidence range defined

140   by the median and standard deviation provided in Table 1, thereby allowing for a reliable year-to-year comparison between 2008 and 2020. Also, table 1 shows that there is no significant change at the global scale of the median when studying seasonal means of cloud covers.

Figure 2 displays the zonal annual mean of the median cloud fraction profile over the 2008–2018 decade and the corresponding standard deviation for the same period. Interannual variability is most pronounced in high-altitude clouds near the equator

145   and in low-level clouds (below 3 km altitude) across all latitudes. These regions generally correspond to areas with higher cloud fractions, where global values always exceed 15% and can locally surpass 35%. Then, figure 4 presents the zonal profiles of annual mean cloud fraction for the year 2008 (a), for 2020 (b), and the difference between the two (c). As in Figure 2, the shaded areas indicate latitudes and altitudes where the values for these specific years are not representative of the 2008–2018
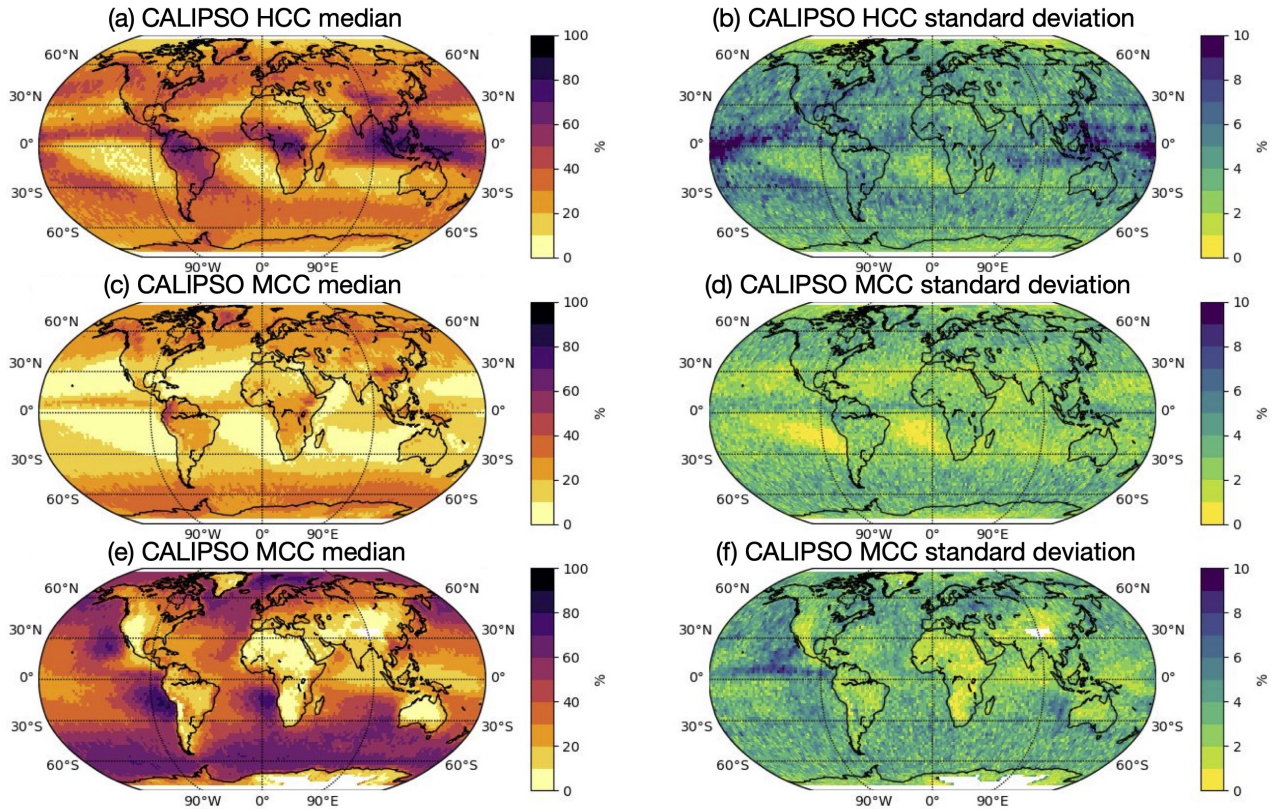
Figure 1. High (a,b) mid (c,d) and low (e,f) yearly means of cloud covers medians (left column) and standard deviations (right column) by CALIPSO between 2008 and 2018. HCC = High Cloud Cover (P < 440 hPa), MCC = Mid Cloud Cover (440 < P < 680 hPa), LCC = Low Cloud Cover (P > 680 hPa).

decadal average. The Arctic low levels cloud fractions appear to be quite different between 2008 and 2020, but except for the region between 25°S and 5°S (and above 14000 m altitude) - affected throughout the atmospheric column by the instrumental issue previously mentioned - all cloud fraction values for 2008 and 2020 are considered statistically significant.

It is important to note, in the context of our comparison between 2008 and 2020, that both years correspond to La Niña conditions, which makes them comparable in terms of cloud cover, particularly over the Pacific Ocean.

3 Model clouds seen from 2 different space lidars

3.1 The COSP-LIDAR algorithm: basics and references

The CFMIP Observation Simulator Package (COSP) is a tool designed to generate synthetic observations from remote sensing instruments by using model output variables as inputs. This approach avoids discrepancies in variable definitions and spatial
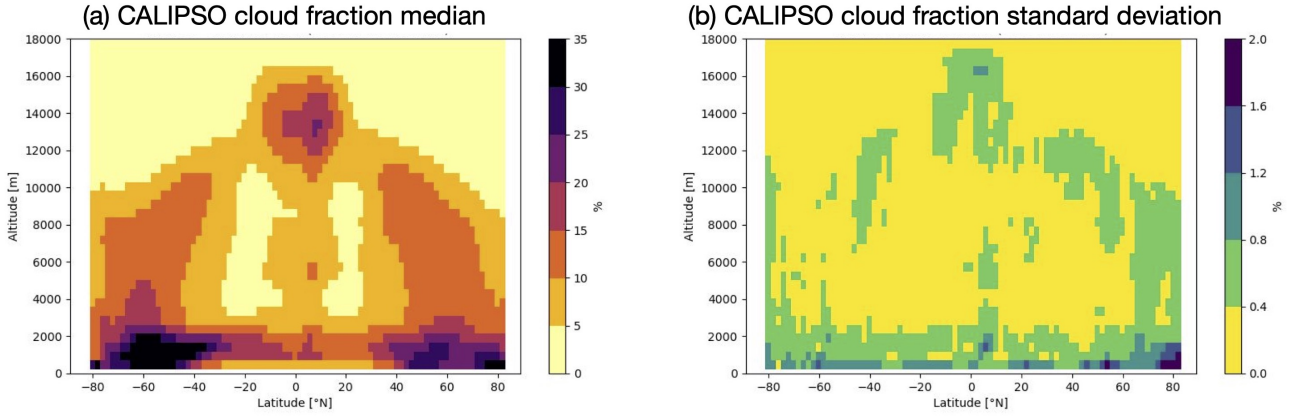
Figure 2. Zonal mean of yearly mean of (a) median and (b) standard deviation cloud fraction by CALIPSO between 2008 and 2018
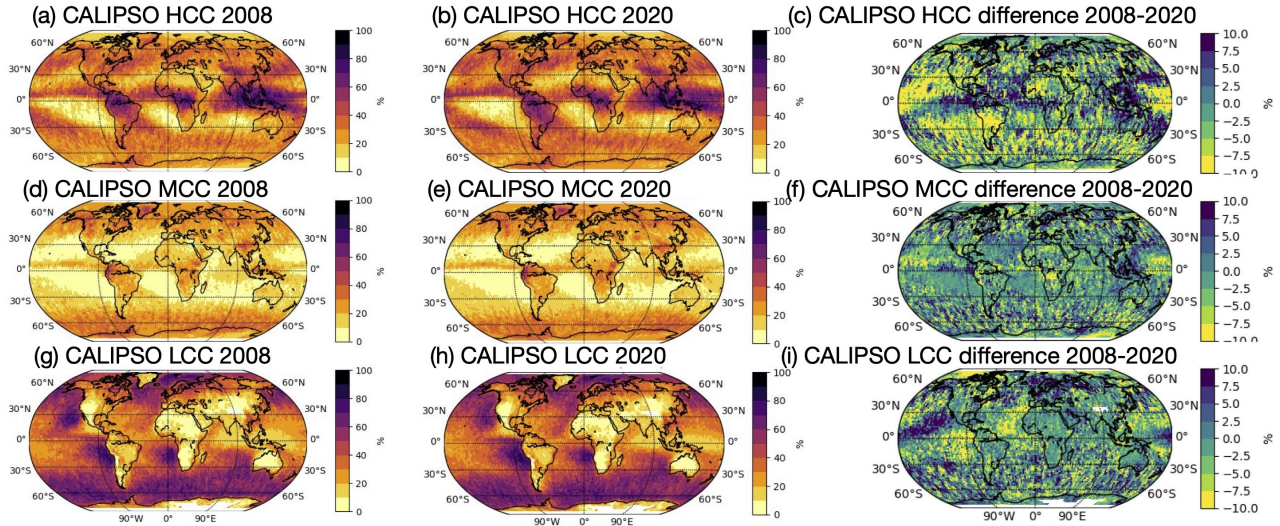
Figure 3. High (a,b,c) mid (d,e,f) low (g,h,i) cloud covers for 2008 (left column), 2020 (middle column) and 2008-2020 difference (right column) by CALIPSO. Grey zones indicate not significant areas (where cloud cover difference is higher than the 2008-2020 mean + 3 standard deviation). HCC = High Cloud Cover (P < 440 hPa), MCC = Mid Cloud Cover (440 < P < 680 hPa), LCC = Low Cloud Cover (P > 680 hPa).

resolution that typically arise when comparing model outputs with instrument measurements. Bodas-Salcedo et al. 2011 details the main steps involved in the algorithm. COSP can also be implemented directly within GCMs, as described in Swales et al. 160 (2018). The interface of COSP is modular and adaptable to a wide range of satellite or in-situ instruments, and it has evolved with successive developments across versions 1 and 2 enabling broader applications.
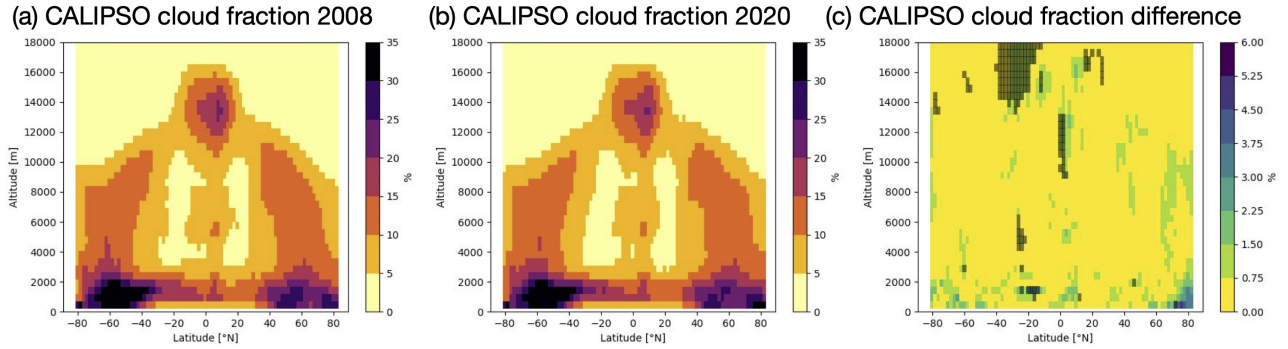
Figure 4. Zonal mean of yearly means of cloud fraction in (a) 2008 (b) 2020, and the (c) 2008-2020 difference, by CALIPSO. Grey zones indicate not significant areas (where cloud fraction difference is higher than the 2008-2020 mean + 3 standard deviation)

The lidar simulation component (COSP-lidar) was initially developed to replicate measurements from CALIOP, the lidar onboard the CALIPSO satellite (Chiriaco et al., 2006; Chepfer et al., 2007). Over time, it has been enhanced to better mimic specific instrument capabilities, including cloud fraction and 3D cloud structure (Chepfer et al., 2008), cloud phase differentia-
165   tion (Cesana and Chepfer, 2013), opaque cloud detection (Guzman et al., 2017), and aerosol characterization (Bonazzola et al., 2023). For spaceborne lidar applications, COSP provides a crucial framework for scale-aware and definition-consistent comparisons between modeled and observed cloud properties, particularly valuable for building long-term multi-lidar simulation datasets. It has already been extensively used to evaluate cloud representation in various models, including those participating in CMIP5 and CMIP6, facilitating consistent multi-model analyses and comparisons with observations (Nam et al., 2014;
170   Williams and Bodas-Salcedo, 2017; Morrison et al., 2019; Kay et al., 2012; Konsta et al., 2022; Cesana et al., 2024).

3.2 Model outputs from LMDZ / IPSL-CM6-LR

In this study, we employed the offline version of COSP, which involves driving the simulator using output variables from a climate model. We selected the model developed by IPSL at the lowest resolution (143 x 144 x 79 grid corresponding to a 200 km horizontal resolution) for the whole 2008 year in the CMIP6 amip experiment (IPSL-CM6-LR, (Eyring et al., 2016))
175   made available on the database of the spirit cluster (see https://esgf-node.ipsl.upmc.fr/search/cmip6-ipsl/), at CF3hr or CFday frequency (depending on the availability of the variables - see next table for details). All the variables at CF3hr frequency have been averaged to get a uniform daily dataset as input for COSP simulations. Table A2 in appendix lists all the variables required to run the lidar simulator, along with their descriptions, dimensions, and the corresponding variable names in the different environments. Some variables that have been put to zero in input of COSP because they are not necessary in the lidar
180   simulation (and not present in the CMIP6 database for the IPSL-CM6-LR model): *mr_ozone*, *dtau_s*, *dtau_c*, *dem_s*, *dem_c*.

3.3 New developments in COSP-LIDAR for AEOLUS

Building on previous developments that enabled optical computations in the cloud module at the 355 nm wavelength for preparing the lidar on board the EarthCARE satellite, ATLID, (Reverdy et al., 2015; Feofilov et al., 2023) we have extended the algorithm to support the ALADIN instrument onboard AEOLUS. Since both ATLID and ALADIN operate at the same wavelength, we can reuse most of the parameter definitions, especially optical parameters, previously established for 355 nm. However, it was necessary to adjust the cloud detection threshold S, which differs between instruments due to their respective sensitivities and horizontal resolutions, as well as the multiple scattering coefficient n. In the case of AEOLUS, the instrument's Line of Sight (LOS) - with an inclination of i = 35° - also must be taken into account in the cloud-related calculations because the laser beam travels through a longer atmospheric path compared to a vertical observation. To accurately simulate the instrument's measurements in the COSP algorithm, we have to replicate the instrument geometry. Therefore, variables 1 to 4 in the table A2 in appendix are multiplied by $1/\cos(35°)$ to adjust for the longer optical path caused by the inclination. The following section (3.4) examines the influences of these parameters (wavelength, inclination, cloud detection threshold, multiple scattering coefficient) on the outputs generated by the lidar simulation. More information on the developments are given in Appendix in table A1.

3.4 Sensitivity tests in COSP-LIDAR

In this section we address the topic of the influence of adjustable parameters related to cloud computation in COSP-lidar. We conducted simulations using input data (for the full 2008 year) from the IPSL-CM6-LR model and modifying for each simulation one of the following parameters in the COSP algorithm: the laser inclination **i**, the multiple scattering coefficient **n**, the cloud detection threshold **S**.

3.4.1 Laser inclination

Figure 5nillustrate the impact of the inclination angle when switching from the left to the right column on the annually averaged cloud fraction simulated for a lidar operating at 355 nm, with a fixed multiple scattering coefficient of η=0.9 and a fixed detection threshold of S=1.84. Red (respectively blue) indicates a positive (respectively negative) difference in cloud fraction with respect to the simulation of reference (chosen with i=35). As AEOLUS measurements are performed at an off-nadir angle, the laser signal travels a longer optical path through the atmosphere. This increased path length leads to greater signal attenuation, resulting in a lower attenuated backscatter (ATB) thus to a lower cloud fraction measured compared to CALIPSO without inclination of the instrument. This is consistent with the slightly higher (between 0 and 3%) cloud fraction simulated at all altitudes when the 35° inclination is removed, except for low level clouds around 2000 m altitude. We particularly want to highlight the fact that the inclination does not alter the global spatial distribution of clouds.
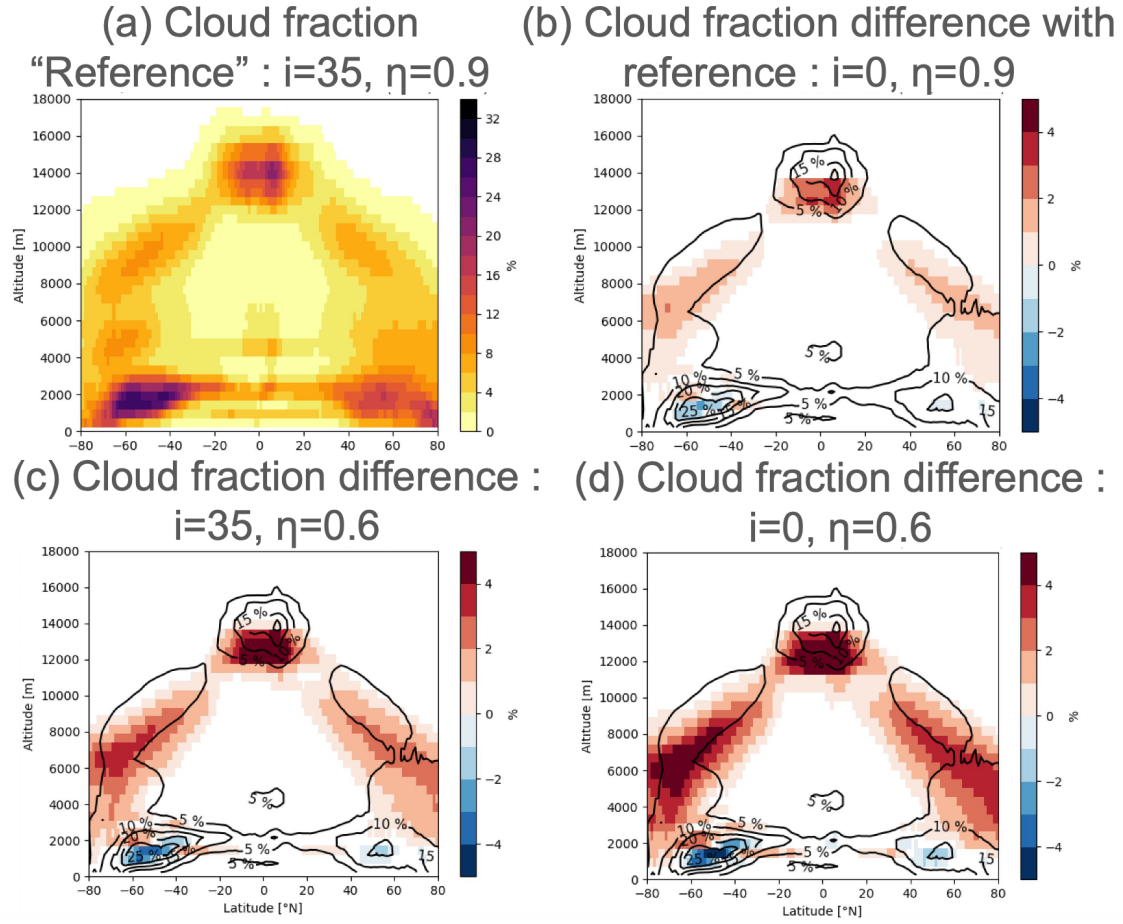
Figure 5. Influence of the inclination (i) and multiple scattering coefficient (η) on the cloud fraction. Cloud fraction lower than 0.1 (for the reference) and absolute values of cloud fraction difference lower than 0.5 are masked.

3.4.2 Multiple scattering coefficient

The difference of the values of the multiple scattering coefficient between two instruments is primarily due to their various instrumental characteristics, such as footprint size and receiver field of view. η=1 corresponds to single scattering and this value is decreasing as the effect of multiple scattering increases. For CALIPSO, the value of n has been previously investigated and set to η=0.7 in COSP-lidar/CALIPSO (Garnier et al., 2015). In the literature, the selected values respectively for EarthCARE/ATLID and AEOLUS are η=0.6 and η=0.9 (Reverdy et al., 2015; Feofilov et al., 2024).

Figure 5 (c) shows that the influence of the multiple scattering coefficient modification, with a fixed inclination of i=35° and a fixed cloud detection threshold of S=1.84 (see Section 3.3.c), is bigger than the one of the inclination. The simulated cloud fraction also decreases at all altitudes when the multiple scattering coefficient increases from η=0.6 to η=0.9, except in the lower atmospheric layers below 2000 m altitude, where cloud fraction values exceed 25%. Above 3000 m altitude, the

Global mean	i=35, η =0.9 λ =355 AEOLUS	i=35, η =0.6 λ =355	i=0, η =0.6 λ =355 EarthCARE/ATLID	i=0, η =0.9 λ =355	i=0, η=0.7 λ=532 CALIPSO
High cloud cover	**13%**	14%	**14%**	14%	**14%**
Mid cloud cover	**15%**	17%	**18%**	16%	**18%**
Low cloud cover	**39%**	40%	**40%**	39%	**40%**

Table 2. Global mean of high/mid/low cloud covers with various configurations of inclination, multiple scattering coefficient and wavelength (with fixed S=1.84 for the 355 nm simulation and S=5.0 for the 532 nm simulation)

reduction in cloud fraction ranges from approximately 2% to 5%. Figure 5 (d) confirms that the impact of simultaneously varying both parameters is consistent with the cumulative effect of their individual contributions observed previously. This last configuration (i = 0, η= 0.6, λ=355 nm) is representative of a simulation closely matching the measurement conditions of the ATLID instrument. Finally, Table 2 details the global annual means of high, mid, and low-level cloud covers for the various tested configurations, in which the inclination and the multiple scattering coefficient are added independently, while keeping the detection threshold and wavelength fixed (S= 1.84 and λ= 355 nm). The last column, corresponding to a simulated configuration closely matching CALIPSO observational conditions, is included for reference. The results indicate that introducing both the inclination and the increase in the multiple scattering coefficient lead to a decrease in cloud cover values by approximately 1 to 3%.

3.4.3 Detection threshold (horizontal resolution)

In the COSP-lidar algorithm, a fixed value s0 of scattering ratio (SR) is used as a threshold to identify cloudy layers (layers with SR>s0 are flagged cloudy). Simulations are performed using a reference cloud detection threshold value of s0=1.84 in COSP-lidar/AEOLUS, as well as scaled values of s0 (0.75 × s0, 1.25 × s0 , 1.5 × s0 and 2 × s0). We set the multiple scattering coefficient to η=0.9 and the inclination of i=35° to replicate the measurements conditions of AEOLUS in all the simulations presented in this paragraph. The choice of s0=1.84 for AEOLUS is motivated by its operating conditions, measuring during the transition between day and night. Additionally, its 355 nm wavelength leads to an attenuated molecular backscatter signal that is approximately five times lower than that observed at 532 nm (as by CALIPSO). This is due to the fact that the molecular attenuated backscatter (*ATB_mol*) is inversely proportional to the fourth power of the wavelength, in accordance with Rayleigh scattering theory. As a result, the scattering ratio (*SR = ATB / ATB_mol*) at 355 nm is about five times smaller than at 532 nm, given that the total attenuated backscatter (*ATB*) from cloud particles is insensitive to the wavelength as the particle sizes involved are significantly larger than 355 and 532 nm. Consequently, the appropriate threshold for cloud detection at 355 nm is around 5 times lower than the one at 532 nm. This threshold value is supported by the analysis of (Reverdy et al., 2015), who estimated the cloud detection threshold for ATLID—operating at the same wavelength under nighttime (sS=1.84) conditions.

Figure 6 presents the differences in cloud fraction obtained from various simulations as the cloud detection threshold varies, with respect to the reference threshold s0=1.84. Simulations using bigger thresholds than s0 reveal that increasing this pa-
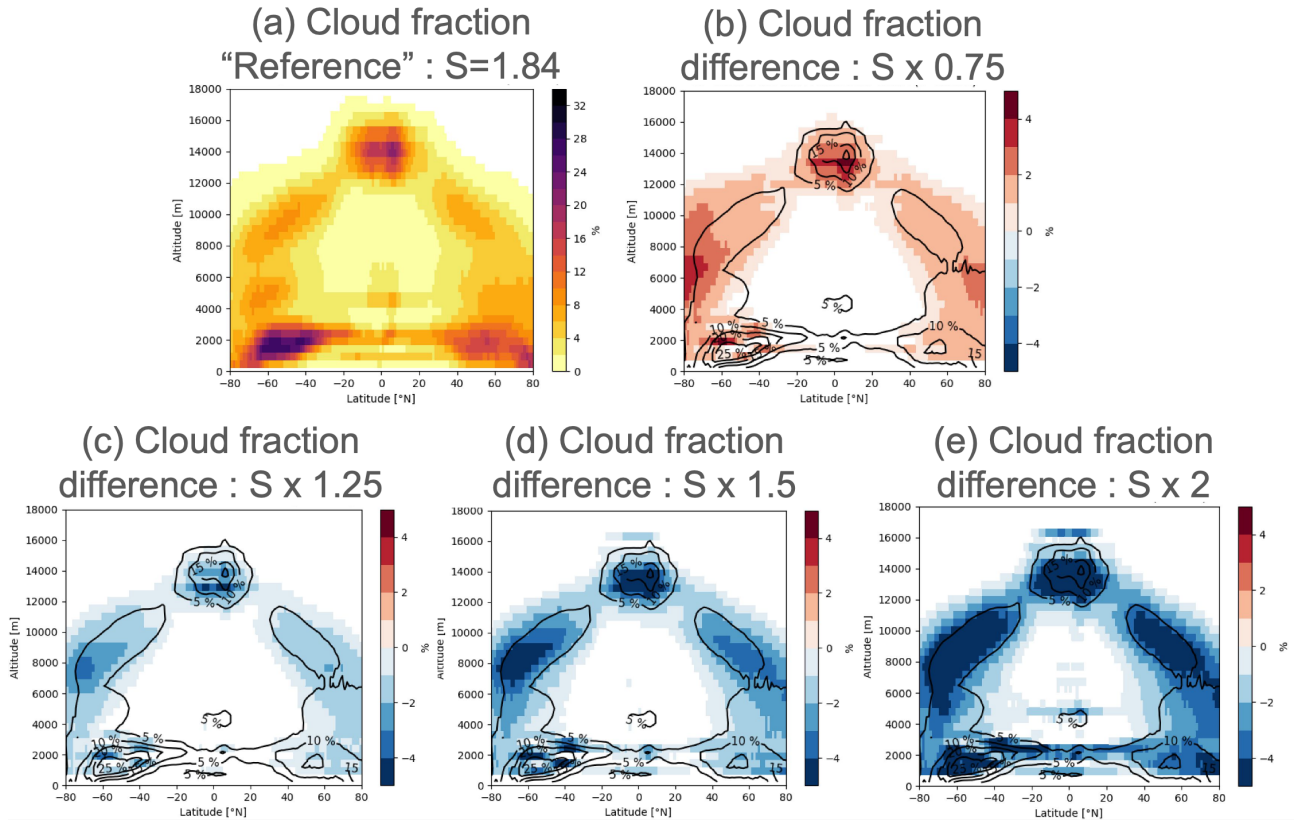
Figure 6. Influence of the cloud detection threshold (S). Cloud fraction lower than 0.1 and absolute values of cloud fraction difference lower than 0.5 are masked.

rameter leads to a systematic reduction in cloud fraction, both horizontally across the globe and vertically throughout the atmospheric column. This decrease is particularly pronounced in regions characterized by high cloud fractions, in the lower troposphere (around 2000 m altitude) at latitudes between 60° and 40°, and at higher altitudes (around 14000 m altitude) near the equator. Only the simulation using a detection threshold lower than s0 (see figure 6 (b)) exhibits an overall increase in cloud fraction. The analysis of cloud cover at high, mid, and low altitudes confirms the result: increasing the detection threshold leads to a reduction in cloud cover across all altitude levels uniformly. This result is expected as a higher cloud detection threshold implies that less small attenuated backscatter signals are identified, leading to a lower measured cloud fraction and potentially to undetected clouds. It is also observed that further increasing the threshold has a limited impact on the results, whereas even a slight decrease in the threshold induces a more significant effect. For instance, multiplying the cloud detection threshold by 0.75 produces a change in cloud cover of similar magnitude to that resulting from multiplying by a factor of 1.5, meaning that LMDZ produces a lot of optically thin clouds.

In conclusion to these sensibility tests, we choose for the COSP-lidar/AEOLUS algorithm to keep the parameters $\eta = 0.9$ and S=1.84 as prescribed in the literature (Reverdy et al., 2015; Feofilov et al., 2022) The results presented in the following

Global mean	s0 x 0.75	**S=1.84**	s0 x 1.25	s0 x 1.5	s0 x 2
High cloud cover	15% (+2)	**13%**	12% (-1)	10% (-3)	7.4% (-5.6)
Mid cloud cover	17% (+2)	**15%**	14% (-1)	12% (-3)	11% (-4)
Low cloud cover	41% (+2)	**39%**	38% (-1)	37% (-2)	33% (-6)

Table 3. Global mean of high/mid/low cloud covers with various configurations of cloud detection threshold

Global mean	COSP-lidar /AEOLUS	COSP-lidar /CALIPSO	OBS AEOLUS	OBS CALIPSO	COSP-lidar /AEOLUS - OBS AEOLUS	COSP-lidar /CALIPSO - OBS CALIPSO	COSP-lidar /AEOLUS - COSP-lidar /CALIPSO	OBS AEOLUS - OBS CALIPSO
High cloud cover	13%	14%	24 %	30%	-11 %	-16%	-1%	-6 %
Mid cloud cover	14%	17%	19%	20%	-5%	-3%	-3%	-1 %
Low cloud cover	38%	38%	44 %	39%	-6 %	-1%	-	+5 %

Table 4. Global mean of high/mid/low cloud covers from COSP simulations and observations for AEOLUS and CALIPSO, and their differences

part of this article are based on the simulation performed using this configuration, which incorporates these parameters with a wavelength of λ=355 nm and a i=35° instrument inclination, to accurately represent the measurements conditions of AEOLUS. While we acknowledge that the selection of these parameters influences the simulated cloud properties, their impact remains limited when compared to the magnitude and temporal variability of the variables we analyzed.

4 Results

In this section, we assess whether the evaluation of cloud representation in the IPSL-CM6-LR model using the COSP-lidar simulator remains robust when based on observations from either CALIPSO or AEOLUS. First, we compared one year of observations from CALIPSO (2008) and AEOLUS (2020) to identify the main differences between the two measurement datasets, including those arising from their respective instrument configurations and measurement conditions. Second, we analyzed the COSP-lidar simulations of the two configurations (COSP-lidar/CALIPSO and COSP-lidar/AEOLUS), in order to isolate differences due to the instrument designs. Finally, we evaluate the LMDZ model performance separately using CALIPSO and AEOLUS observations, and compare the resulting mode-to–observation discrepancies. This step accounts for both instrument-specific effects and the influence of interannual variability that have been previously discussed, aiming to determine whether cloud diagnostics derived from AEOLUS can be reliably used as CALIPSO for climate model evaluation.
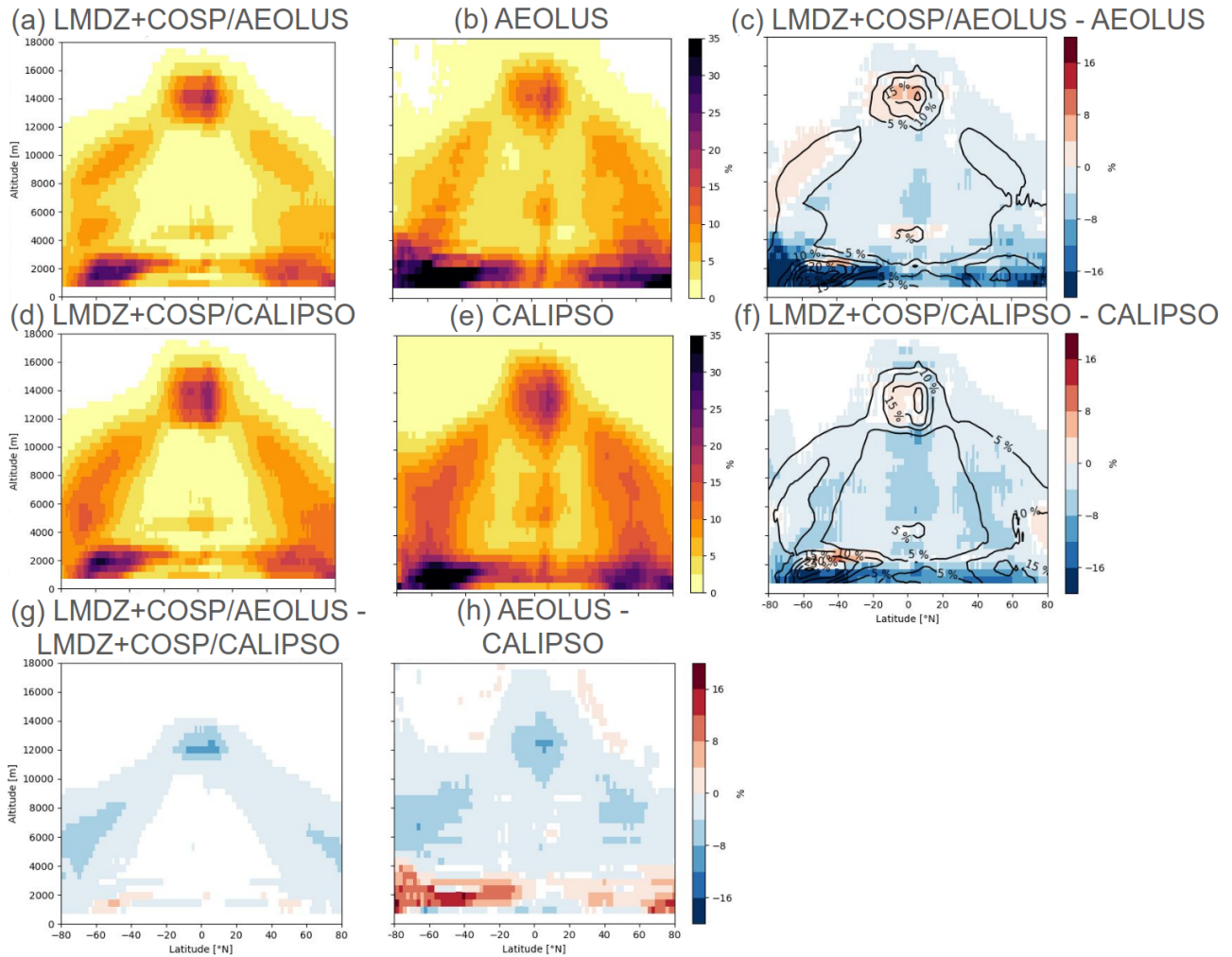
Figure 7. Zonal means of cloud fraction for (a) LMDZ+COSP/AEOLUS, (b) AEOLUS (2020), (d) LMDZ+COSP/CALIPSO, (e) CALIPSO (2008), model-to-observations differences for (c) AEOLUS and (f) CALIPSO, model-to-model difference (g) between LMDZ+COSP AEOLUS and CALIPSO simulations, and observational difference (h) between AEOLUS and CALIPSO measurements. Cloud fractions smaller than 0.1% and absolute values of cloud fractions differences smaller than 0.5% are masked.

4.1 AEOLUS vs CALIPSO observations

Figure 7 - middle column presents the zonal mean cloud fraction profiles derived from CALIPSO measurements in 2008 and AEOLUS observations in 2020, and their difference. Several key differences between AEOLUS and CALIPSO designs can lead to discrepancies in cloud detection that must be accounted for when comparing their retrievals. Firstly, AEOLUS uses a shorter wavelength than CALIPSO (Hunt et al., 2009) and CALIPSO is sensitive to polarization unlike AEOLUS - for which climatological depolarization ratios are used to compensate for better discrimination of cloud phase. Also, as we address
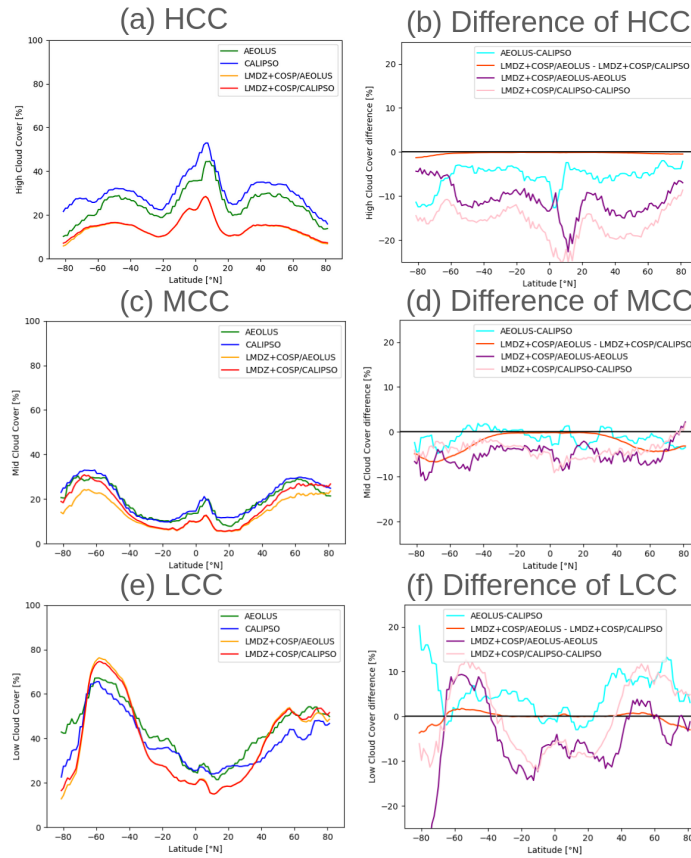
Figure 8. Zonal mean of yearly means of cloud covers and model-to-observations and model-to-model differences, at high (a,b) mid (c,d) and low (e,f) levels for AEOLUS and CALIPSO

in Section 3.3.a, their viewing geometries differ. Furthermore, CALIPSO and AEOLUS have limited co-locations due to their equatorial crossing times, which also introduces differences related to the diurnal cycle of clouds (Feofilov et al., 2024; Chepfer et al., 2019; Noel et al., 2018). To address this, a correction using diurnal variability observed by the CATS (Cloud–Aerosol Transport System) lidar onboard the ISS (International Space Station) could be used (Feofilov et al., 2024; Titus et al., 2025), but we are not applying it in this study. The coarser horizontal resolution of AEOLUS can also play a role as it can lead to artificial increased cloud fraction due to the instrument's along orbit track resolution (Titus et al., 2025) especially in regions with sparse low level clouds that are seen as overcasted. AEOLUS averages the signal over larger volumes that can lead to a merge of smaller cloud signals, thus reducing the instrument's ability to detect small or thin cloud features.

The coarser horizontal resolution of AEOLUS further reduces sensitivity to small-scale clouds, particularly trade cumulus, for which cloud fraction can be underestimated by up to 25% (Chepfer et al., 2013).

A systematic larger cloud fraction (shown in red) by AEOLUS around 2000 m altitude, that is bigger in the Southern Hemisphere, ranging from 8 to 20% (vs less than 12% in the Northern Hemisphere). This bias is consistent with expectations,

Global mean	COSP-lidar /AEOLUS	COSP-lidar /CALIPSO	OBS AEOLUS	OBS CALIPSO	COSP-lidar /AEOLUS - OBS AEOLUS	COSP-lidar /CALIPSO - OBS CALIPSO	COSP-lidar /AEOLUS - COSP-lidar /CALIPSO	OBS AEOLUS - OBS CALIPSO
High cloud cover	13%	14%	24%	27%	-11%	-13%	-1%	-3 %
Mid cloud cover	4.1%	4.3%	8.9%	8.5%	-4.8 %	-4.2%	-0.2%	+0.4%
Low cloud cover	21%	21%	35%	34%	-24%	-23%	-	+1 %

Table 5. Spatial mean in cumulus regions of high/mid/low cloud covers from COSP simulations and observations for AEOLUS and CALIPSO, and their differences

Global mean	COSP-lidar /AEOLUS	COSP-lidar /CALIPSO	OBS AEOLUS	OBS CALIPSO	COSP-lidar /AEOLUS - OBS AEOLUS	COSP-lidar /CALIPSO - OBS CALIPSO	COSP-lidar /AEOLUS - COSP-lidar /CALIPSO	OBS AEOLUS - OBS CALIPSO
High cloud cover	6.8%	6.8%	16 %	19%	-9.2%	-12.2%	-	-3 %
Mid cloud cover	3.8%	4.1%	6.4 %	6.5%	-2.6%	-2.4%	-0.3%	+0.1%
Low cloud cover	44%	44%	52 %	51%	-8 %	-7%	-	+1 %

Table 6. Spatial mean in stratocumulus regions of high/mid/low cloud covers from COSP simulations and observations for AEOLUS and CALIPSO, and their differences

as it likely results from the coarser spatial resolution of AEOLUS (3 km along the orbit track) compared to the finer horizontal sampling of CALIPSO (330 m) Two regions with smaller cloud fractions observed by AEOLUS (from 4 to 8%) are located between 40° and 60° in both hemispheres between 4000 and 10000 m. As shown in the previous sensitivity tests (see Figure 5), this difference may result from the effects of viewing angle or multiple scattering. Elsewhere, the differences between the two lidars are less than 4% in absolute value and can be biased by interannual variability, as the observational years being compared are not the same.

Global mean	COSP-lidar /AEOLUS	COSP-lidar /CALIPSO	OBS AEOLUS	OBS CALIPSO	COSP-lidar /AEOLUS - OBS AEOLUS	COSP-lidar /CALIPSO - OBS CALIPSO	COSP-lidar /AEOLUS - COSP-lidar /CALIPSO	OBS AEOLUS - OBS CALIPSO
High cloud cover	17%	17%	32 %	35%	-15 %	-18%	-	-1 %
Mid cloud cover	7.4%	7.8%	13 %	14%	-5.6 %	-6.2%	-0.4%	-3 %
Low cloud cover	9.2%	9.3%	19%	19%	-9.8%	-9.7%	-0.1%	-

Table 7. Spatial mean in the Indian Ocean region of high/mid/low cloud covers from COSP simulations and observations for AEOLUS and CALIPSO, and their differences

Global mean	COSP-lidar /AEOLUS	COSP-lidar /CALIPSO	OBS AEOLUS	OBS CALIPSO	COSP-lidar /AEOLUS - OBS AEOLUS	COSP-lidar /CALIPSO - OBS CALIPSO	COSP-lidar /AEOLUS - COSP-lidar /CALIPSO	OBS AEOLUS - OBS CALIPSO
High cloud cover	32%	32%	49 %	56%	-18 %	-24%	-	-6%
Mid cloud cover	10%	10%	15%	17%	-2%	-7%	-	-5 %
Low cloud cover	10%	10%	20 %	21%	-10 %	-11%	-	-1 %

Table 8. Spatial mean in the Warm Pool region of high/mid/low cloud covers from COSP simulations and observations for AEOLUS and CALIPSO, and their differences

4.2 COSP-lidar/AEOLUS vs COSP-lidar/CALIPSO simulations

The differences between cloud fractions simulated using the AEOLUS and CALIPSO configurations are all below 10% in absolute value (Figure 7 (g)). Overall, the COSP-lidar/AEOLUS simulations produce lower cloud fractions (mostly around 4%) at all altitudes except in the low levels with respect to COSP-lidar/CALIPSO ones.

300   Figure 7 (g) is consistent with the sensitivity tests previously conducted (see Figure 5). It highlights the difference between the COSP-lidar/AEOLUS simulation configured with a wavelength of 355 nm, a multiple scattering efficiency factor η = 0.9, and a viewing angle inclination of 35°, and the COSP-lidar/CALIPSO simulation using a wavelength of 532 nm, η = 0.7, and no inclination. In this case, the combined effects of a reduced multiple scattering coefficient and the absence of inclination result in a negative difference of approximately 4% in cloud fraction for mid-level clouds (between 4000 and 10000 m) beyond 20°

305   latitude and towards the poles. A positive difference in low-level cloud fraction, particularly over the Southern Hemisphere, is also observed, ranging from 4% to 6%. This difference arises from the specific characteristics of each instrument we accounted for in the COSP-lidar algorithm (e.g. viewing angle and multiple scattering coefficient) as demonstrated by the sensitivity tests to various parameters presented in Section 3.3.

4.3 (MOD-OBS) AEOLUS vs (MOD-OBS) CALIPSO results and analysis

310   The model–observation differences for each instrument allow us to assess whether the model evaluation remains consistent regardless of the lidar used, provided that the COSP-lidar tool is appropriately configured and taking account of the actual discrepancies between the two observational datasets. The previous comparisons demonstrated that the discrepancy between COSP-lidar/AEOLUS and COSP-lidar/CALIPSO (Figure 7 (g)) is consistent with the difference observed between the respective lidar measurements (Figure 7 (h)), particularly in the middle and upper troposphere, showing a small (around 4% and

315   maximum 10%) underestimation of the cloud fraction for AEOLUS with respect to CALIPSO at every latitudes and altitudes. Cesana et al. (2022) identified cloud phase and vertical distribution biases in CMIP6 models, which are consistent with the cloud fraction biases we observe in our analysis. Similar spatial patterns emerge, suggesting that these biases persist across datasets. The model evaluation presented in the figures 7 (c) and (f) share common features: a slight overestimation of high level cloud fractions near 13000 m at the equator (4-8%) by the model and a substantial underestimation of low level cloud

320   fractions below 2000 m (more than 10%) across all latitudes but bigger in the Southern hemisphere (reaching up to 20%) by the model. This underestimation is particularly high in cumulus and stratocumulus regions with a low cloud cover bias higher in these areas (between 7 and 23%) than at the global scale (between 1 and 7%) (see tables 6, 7, 8). In the case of CALIPSO, it should be noted that the model-observation difference can be affected by interannual variability but only by a few percent (from 0.5 to 2%). It is crucial to highlight the negligible magnitude of the discrepancies linked to configuration differences (presented

325   in Section 4.2) in comparison with the amplitude of the model bias. Madeleine et al. (2020) reported an overestimation of low-level cloud cover in the 30–60° latitude band of both hemispheres in IPSL-CM6A-LR, along with a general underestimation elsewhere, based on comparisons with CALIPSO observations. Our results, illustrated in Figure 7 (g), corroborate these findings. In addition, we find that low and high-level cloud covers are globally underestimated in IPSL-CM6A-LR, especially in the warm pool region by 11 to 24% (see tables 4 and 8).

330   Figure 7 (h) shows the differences between observational datasets from AEOLUS and CALIPSO. It is reassuring to observe the recurrence of similar patterns as in Figure 7 (g) : a negative difference around 12000 m at the equator, a negative difference between 4000 and 1000 m beyond 20° latitude toward the poles, and a positive difference near 2000 m altitude, consistent across all longitudes but more pronounced in the Southern Hemisphere. This suggests that the simulations realistically reproduce the observed differences between the two instruments, which result from their respective measurement configurations.

5 Conclusion and perspectives

This study highlights that despite AEOLUS not being designed for cloud measurements, its observations can serve like those of CALIPSO as a valuable tool for evaluating cloud representation in General Circulation Models (GCMs). There is no major difference (less than 4%) between the simulated cloud covers for AEOLUS (COSP-lidar/AEOLUS) and CALIPSO (COSP-lidar/CALIPSO) configurations. We made sensitivity tests which explained that those small discrepancies are due to viewing geometry, multiple scattering and sensivity (cloud detection threshold) differences between the two instruments. On the observational side, comparisons between AEOLUS and CALIPSO measurements over a one-year period also reveal small differences in cloud cover (less than 10%). These model-to-model and observation-to-observation differences are negligible with respect to model biases. These ones have been re-assessed : there is a significant underestimation of cloud fractions at low levels in the LMDZ model, which can be underestimated with more than 20% bias (particularly in cumulus regions and in the southern hemisphere). High-altitude clouds are also underestimated in specific regions such as the warm pool where the cloud cover negative bias can reach up to 20%. These findings underline the need for improved observational constraints and model parametrizations for clouds and support the fact that model evaluations using AEOLUS are consistent to those using CALIPSO.

Looking ahead, a key challenge lies in merging long-term datasets from multiple spaceborne lidars, incorporating successively CALIPSO (2006-2023), AEOLUS (2018-2023) and ATLID (since 2024). This requires harmonized processing strategies for the measurements datasets and adapted configurations of the COSP-lidar tool to ensure continuity across the instruments for reliable multi-decades model-to-observation comparisons. As we successfully developed the AEOLUS module in COSP - used here as a reference for EarthCARE/ATLID due to their shared characteristics and the temporal overlap in measurements with CALIPSO - future work will focus on refining again the COSP-lidar algorithm to perform similar simulations for Earth-CARE/ATLID. We aim to establish a comprehensive multi-lidar comparison with CMIP6 model outputs of cloud observations from CALIPSO to EarthCARE/ATLID. Furthermore, since ATLID is specifically designed for cloud detection and offers a fine vertical resolution, similar cloud-related biases in the model are expected to be observed with potentially greater amplitudes.

Additionally, AEOLUS wind measurements (not used in the current study) offer a unique opportunity in future work to assess the vertical and global performance of modelled winds, and to explore cloud-wind interactions in GCMs through the COSP/AEOLUS framework.

Code availability. The updated version of the COSP-lidar algorithm, including the developments related to AEOLUS will be made publicly available on the official COSP GitHub repository upon publication of the article.

Author contributions. MLR and HC conceived and designed the study. Data collection was performed by MLR and ZT. All the authors interpreted the results. The manuscript was written by MLR and HC with input from all co-authors.

365 *Competing interests.* The authors declare that they have no conflict of interest.

Acknowledgements. The authors thank NASA and CNES for providing CALIPSO satellite data and ESA for providing AEOLUS satellite data. We acknowledge the CNRS for the funding of MLR.

References

Bodas-Salcedo, A., Webb, M. J., Bony, S., Chepfer, H., Dufresne, J.-L., Klein, S. A., Zhang, Y., Marchand, R., Haynes, J. M., Pincus, R., and John, V. O.: COSP: Satellite simulation software for model assessment, Bulletin of the American Meteorological Society, 92, 1023 – 1043, https://doi.org/10.1175/2011BAMS2856.1, 2011.

Bonazzola, M., Chepfer, H., Ma, P.-L., Quaas, J., Winker, D. M., Feofilov, A., and Schutgens, N.: Incorporation of aerosol into the COSPv2 satellite lidar simulator for climate model evaluation, Geoscientific Model Development, 16, 1359–1377, https://doi.org/10.5194/gmd-16-1359-2023, 2023.

Bony, S. and Dufresne, J.-L.: Marine boundary layer clouds at the heart of tropical cloud feedback uncertainties in climate models, Geophysical Research Letters, 32, https://doi.org/https://doi.org/10.1029/2005GL023851, 2005.

Boucher, O., Servonnat, J., Albright, A. L., Aumont, O., Balkanski, Y., Bastrikov, V., Bekki, S., Bonnet, R., Bony, S., Bopp, L., Braconnot, P., Brockmann, P., Cadule, P., Caubel, A., Cheruy, F., Codron, F., Cozic, A., Cugnet, D., D'Andrea, F., Davini, P., de Lavergne, C., Denvil, S., Deshayes, J., Devilliers, M., Ducharne, A., Dufresne, J.-L., Dupont, E., Éthé, C., Fairhead, L., Falletti, L., Flavoni, S., Foujols, M.-A., Gardoll, S., Gastineau, G., Ghattas, J., Grandpeix, J.-Y., Guenet, B., Guez, Lionel, E., Guilyardi, E., Guimberteau, M., Hauglustaine, D., Hourdin, F., Idelkadi, A., Joussaume, S., Kageyama, M., Khodri, M., Krinner, G., Lebas, N., Levavasseur, G., Lévy, C., Li, L., Lott, F., Lurton, T., Luyssaert, S., Madec, G., Madeleine, J.-B., Maignan, F., Marchand, M., Marti, O., Mellul, L., Meurdesoif, Y., Mignot, J., Musat, I., Ottlé, C., Peylin, P., Planton, Y., Polcher, J., Rio, C., Rochetin, N., Rousset, C., Sepulchre, P., Sima, A., Swingedouw, D., Thiéblemont, R., Traore, A. K., Vancoppenolle, M., Vial, J., Vialard, J., Viovy, N., and Vuichard, N.: Presentation and Evaluation of the IPSL-CM6A-LR Climate Model, Journal of Advances in Modeling Earth Systems, 12, e2019MS002 010, https://doi.org/https://doi.org/10.1029/2019MS002010, e2019MS002010 10.1029/2019MS002010, 2020.

Cesana, G. and Chepfer, H.: Evaluation of the cloud thermodynamic phase in a climate model using CALIPSO-GOCCP, Journal of Geophysical Research: Atmospheres, 118, 7922–7937, https://doi.org/https://doi.org/10.1002/jgrd.50376, 2013.

Cesana, G. V., Khadir, T., Chepfer, H., and Chiriaco, M.: Southern Ocean Solar Reflection Biases in CMIP6 Models Linked to Cloud Phase and Vertical Structure Representations, Geophysical Research Letters, 49, e2022GL099 777, https://doi.org/https://doi.org/10.1029/2022GL099777, e2022GL099777 2022GL099777, 2022.

Cesana, G. V., Ackerman, A. S., Fridlind, A. M., Silber, I., Del, A. D., Zelinka, M. D., Chepfer, H., Khadir, T., and Roehrig, R.: Observational constraint on a feedback from supercooled clouds reduces projected warming uncertainty, Communications Earth Environment, 5, https://doi.org/10.1038/s43247-024-01339-1, 2024.

Chepfer, H., Chiriaco, M., Vautard, R., and Spinhirne, J.: Evaluation of MM5 Optically Thin Clouds over Europe in Fall Using ICESat Lidar Spaceborne Observations, Monthly Weather Review, 135, 2737 – 2753, https://doi.org/10.1175/MWR3413.1, 2007.

Chepfer, H., Bony, S., Winker, D., Chiriaco, M., Dufresne, J.-L., and Sèze, G.: Use of CALIPSO lidar observations to evaluate the cloudiness simulated by a climate model, Geophysical Research Letters, 35, https://doi.org/https://doi.org/10.1029/2008GL034207, 2008.

Chepfer, H., Bony, S., Winker, D., Cesana, G., Dufresne, J. L., Minnis, P., Stubenrauch, C. J., and Zeng, S.: The GCM-Oriented CALIPSO Cloud Product (CALIPSO-GOCCP), Journal of Geophysical Research: Atmospheres, 115, https://doi.org/https://doi.org/10.1029/2009JD012251, 2010.

Chepfer, H., Cesana, G., Winker, D., Getzewich, B., Vaughan, M., and Liu, Z.: Comparison of two different cloud climatologies derived from CALIOP-attenuated backscattered measurements (level 1): The calipso-st and the calipso-GOCCP, Journal of Atmospheric and Oceanic Technology, 30, 725–744, https://doi.org/10.1175/jtech-d-12-00057.1, 2013.

405 Chepfer, H., Brogniez, H., and Noel, V.: Diurnal variations of cloud and relative humidity profiles across the tropics, Scientific Reports, 9, https://doi.org/10.1038/s41598-019-52437-6, 2019.

Chepfer, H., Chomette, O., Arouf, A., Noel, V., Winker, D., Feofilov, A., and Alava Baldazo, A.: Variability and Trends in Cloud Properties Over 17 Years From CALIPSO Space Lidar Observations, Journal of Geophysical Research: Atmospheres, 130, e2025JD043 764, https://doi.org/https://doi.org/10.1029/2025JD043764, e2025JD043764 2025JD043764, 2025.

410 Chiriaco, M., Vautard, R., Chepfer, H., Haeffelin, M., Dudhia, J., Wanherdrick, Y., Morille, Y., and Protat, A.: The Ability of MM5 to Simulate Ice Clouds: Systematic Comparison between Simulated and Measured Fluxes and Lidar/Radar Profiles at the SIRTA Atmospheric Observatory, Monthly Weather Review, 134, 897 – 918, https://doi.org/10.1175/MWR3102.1, 2006.

Donovan, D. P., van Zadelhoff, G.-J., and Wang, P.: The EarthCARE lidar cloud and aerosol profile processor (A-PRO): the A-AER, A-EBD, A-TC, and A-ICE products, Atmospheric Measurement Techniques, 17, 5301–5340, https://doi.org/10.5194/amt-17-5301-2024, 2024.

415 Eyring, V., Bony, S., Meehl, G. A., Senior, C. A., Stevens, B., Stouffer, R. J., and Taylor, K. E.: Overview of the Coupled Model Intercomparison Project Phase 6 (CMIP6) experimental design and organization, Geoscientific Model Development, 9, 1937–1958, https://doi.org/10.5194/gmd-9-1937-2016, 2016.

Feofilov, A., Chepfer, H., Noël, V., and Hajiaghazadeh-Roodsari, M.: Towards Establishing a Long-Term Cloud Record from Space-Borne Lidar Observations, Springer aerospace technology, pp. 57–72, https://doi.org/10.1007/978-3-031-53618-2_6, 2024.

420 Feofilov, A. G., Chepfer, H., Noël, V., Guzman, R., Gindre, C., Ma, P.-L., and Chiriaco, M.: Comparison of scattering ratio profiles retrieved from ALADIN/Aeolus and CALIOP/CALIPSO observations and preliminary estimates of cloud fraction profiles, Atmospheric Measurement Techniques, 15, 1055–1074, https://doi.org/10.5194/amt-15-1055-2022, 2022.

Feofilov, A. G., Chepfer, H., Noël, V., and Szczap, F.: Incorporating EarthCARE observations into a multi-lidar cloud climate record: the ATLID (Atmospheric Lidar) cloud climate product, Atmospheric Measurement Techniques, 16, 3363–3390, https://doi.org/10.5194/amt-425 16-3363-2023, 2023.

Flamant, P., Cuesta, J., Denneulin, M.-L., Dabas, A., and Huber, D.: ADM-Aeolus retrieval algorithms for aerosol and cloud products, Tellus A, 60, 273–288, https://doi.org/https://doi.org/10.1111/j.1600-0870.2007.00287.x, 2008.

Garnier, A., Pelon, J., Vaughan, M. A., Winker, D. M., Trepte, C. R., and Dubuisson, P.: Lidar multiple scattering factors inferred from CALIPSO lidar and IIR retrievals of semi-transparent cirrus cloud optical depths over oceans, Atmospheric Measurement Techniques, 8, 430 2759–2774, https://doi.org/10.5194/amt-8-2759-2015, 2015.

Guzman, R., Chepfer, H., Noel, V., Vaillant de Guélis, T., Kay, J. E., Raberanto, P., Cesana, G., Vaughan, M. A., and Winker, D. M.: Direct atmosphere opacity observations from CALIPSO provide new constraints on cloud-radiation interactions, Journal of Geophysical Research: Atmospheres, 122, 1066–1085, https://doi.org/https://doi.org/10.1002/2016JD025946, 2017.

Hourdin, F., Rio, C., Grandpeix, J.-Y., Madeleine, J.-B., Cheruy, F., Rochetin, N., Jam, A., Musat, I., Idelkadi, A., Fairhead, L., Fou-435 jols, M.-A., Mellul, L., Traore, A.-K., Dufresne, J.-L., Boucher, O., Lefebvre, M.-P., Millour, E., Vignon, E., Jouhaud, J., Diallo, F. B., Lott, F., Gastineau, G., Caubel, A., Meurdesoif, Y., and Ghattas, J.: LMDZ6A: The Atmospheric Component of the IPSL Climate Model With Improved and Better Tuned Physics, Journal of Advances in Modeling Earth Systems, 12, e2019MS001 892, https://doi.org/https://doi.org/10.1029/2019MS001892, e2019MS001892 10.1029/2019MS001892, 2020.

Hunt, W. H., Winker, D. M., Vaughan, M. A., Powell, K. A., Lucker, P. L., and Weimer, C.: CALIPSO Lidar Description and Performance 440 Assessment, Journal of Atmospheric and Oceanic Technology, 26, 1214 – 1228, https://doi.org/10.1175/2009JTECHA1223.1, 2009.

Kay, J. E., Hillman, B. R., Klein, S. A., Zhang, Y., Medeiros, B., Pincus, R., Gettelman, A., Eaton, B., Boyle, J., Marchand, R., and Ackerman, T. P.: Exposing Global Cloud Biases in the Community Atmosphere Model (CAM) Using Satellite Observations and Their Corresponding Instrument Simulators, Journal of Climate, 25, 5190 – 5207, https://doi.org/10.1175/JCLI-D-11-00469.1, 2012.

Konsta, D., Dufresne, J.-L., Chepfer, H., Vial, J., Koshiro, T., Kawai, H., Bodas-Salcedo, A., Roehrig, R., Watanabe, M., and Ogura, T.: Low-Level Marine Tropical Clouds in Six CMIP6 Models Are Too Few, Too Bright but Also Too Compact and Too Homogeneous, Geophysical Research Letters, 49, e2021GL097 593, https://doi.org/https://doi.org/10.1029/2021GL097593, e2021GL097593 2021GL097593, 2022.

Madeleine, J.-B., Hourdin, F., Grandpeix, J.-Y., Rio, C., Dufresne, J.-L., Vignon, E., Boucher, O., Konsta, D., Cheruy, F., Musat, I., Idelkadi, A., Fairhead, L., Millour, E., Lefebvre, M.-P., Mellul, L., Rochetin, N., Lemonnier, F., Touzé-Peiffer, L., and Bonazzola, M.: Improved Representation of Clouds in the Atmospheric Component LMDZ6A of the IPSL-CM6A Earth System Model, Journal of Advances in Modeling Earth Systems, 12, e2020MS002 046, https://doi.org/https://doi.org/10.1029/2020MS002046, e2020MS002046 10.1029/2020MS002046, 2020.

Morrison, A. L., Kay, J. E., Frey, W. R., Chepfer, H., and Guzman, R.: Cloud Response to Arctic Sea Ice Loss and Implications for Future Feedback in the CESM1 Climate Model, Journal of Geophysical Research: Atmospheres, 124, 1003–1020, https://doi.org/https://doi.org/10.1029/2018JD029142, 2019.

Nam, C. C. W., Quaas, J., Neggers, R., Siegenthaler-Le Drian, C., and Isotta, F.: Evaluation of boundary layer cloud parameterizations in the ECHAM5 general circulation model using CALIPSO and CloudSat satellite data, Journal of Advances in Modeling Earth Systems, 6, 300–314, https://doi.org/https://doi.org/10.1002/2013MS000277, 2014.

Noel, V., Chepfer, H., Hoareau, C., Reverdy, M., and Cesana, G.: Effects of solar activity on noise in CALIOP profiles above the South Atlantic Anomaly, Atmospheric Measurement Techniques, 7, 1597–1603, https://doi.org/10.5194/amt-7-1597-2014, 2014.

Noel, V., Chepfer, H., Chiriaco, M., and Yorks, J.: The diurnal cycle of cloud profiles over land and ocean between $51°$ S and $51°$ N, seen by the CATS spaceborne lidar from the International Space Station, Atmospheric Chemistry and Physics, 18, 9457–9473, https://doi.org/10.5194/acp-18-9457-2018, 2018.

Reverdy, M., Chepfer, H., Donovan, D., Noel, V., Cesana, G., Hoareau, C., Chiriaco, M., and Bastin, S.: An EarthCARE/ATLID simulator to evaluate cloud description in climate models, Journal of Geophysical Research: Atmospheres, 120, 11,090–11,113, https://doi.org/https://doi.org/10.1002/2015JD023919, 2015.

Sherwood, S. C., Webb, M. J., Annan, J. D., Armour, K. C., Forster, P. M., Hargreaves, J. C., Hegerl, G., Klein, S. A., Marvel, K. D., Rohling, E. J., Watanabe, M., Andrews, T., Braconnot, P., Bretherton, C. S., Foster, G. L., Hausfather, Z., von der Heydt, A. S., Knutti, R., Mauritsen, T., Norris, J. R., Proistosescu, C., Rugenstein, M., Schmidt, G. A., Tokarska, K. B., and Zelinka, M. D.: An Assessment of Earth's Climate Sensitivity Using Multiple Lines of Evidence, Reviews of Geophysics, 58, e2019RG000 678, https://doi.org/https://doi.org/10.1029/2019RG000678, e2019RG000678 2019RG000678, 2020.

Swales, D. J., Pincus, R., and Bodas-Salcedo, A.: The Cloud Feedback Model Intercomparison Project Observational Simulator Package: Version 2, Geoscientific Model Development, 11, 77–81, https://doi.org/10.5194/gmd-11-77-2018, 2018.

Titus, Z.: ALADIN/Aeolus - Wind-cloud interactions dataset, 2024.

Titus, Z., Bonazzola, M., Chepfer, H., Feofilov, A., Roussel, M.-L., Witschas, B., and Bastin, S.: Wind-cloud interactions observed with Aeolus spaceborne Doppler Wind Lidar, EGUsphere, 2025, 1–40, https://doi.org/10.5194/egusphere-2025-2065, 2025.

Vial, J., Dufresne, J.-L., and Bony, S.: On the interpretation of inter-model spread in CMIP5 climate sensitivity estimates, Climate Dynamics, 41, 3339–3362, https://doi.org/10.1007/s00382-013-1725-9, 2013.

Wang, P., Donovan, D. P., van Zadelhoff, G.-J., de Kloe, J., Huber, D., and Reissig, K.: Evaluation of Aeolus feature mask and particle extinction coefficient profile products using CALIPSO data, Atmospheric Measurement Techniques, 17, 5935–5955,

480   https://doi.org/10.5194/amt-17-5935-2024, 2024.

Wehr, T., Kubota, T., Tzeremes, G., Wallace, K., Nakatsuka, H., Ohno, Y., Koopman, R., Rusli, S., Kikuchi, M., Eisinger, M., Tanaka, T., Taga, M., Deghaye, P., Tomita, E., and Bernaerts, D.: The EarthCARE mission – science and system overview, Atmospheric Measurement Techniques, 16, 3581–3608, https://doi.org/10.5194/amt-16-3581-2023, 2023.

Williams, K. D. and Bodas-Salcedo, A.: A multi-diagnostic approach to cloud evaluation, Geoscientific Model Development, 10, 2547–2566,

485   https://doi.org/10.5194/gmd-10-2547-2017, 2017.

Zelinka, M. D., Myers, T. A., McCoy, D. T., Po-Chedley, S., Caldwell, P. M., Ceppi, P., Klein, S. A., and Taylor, K. E.: Causes of Higher Climate Sensitivity in CMIP6 Models, Geophysical Research Letters, 47, e2019GL085 782, https://doi.org/https://doi.org/10.1029/2019GL085782, e2019GL085782 10.1029/2019GL085782, 2020.

	Variable name in COSP	Description
Optical inputs	beta_mol_aeolus	Lidar molecular backscatter coefficient
	betatot_aeolus	Lidar backscatter coefficient
	tau_mol_aeolus	Lidar molecular optical depth
	tautot_aeolus	Lidar molecular optical depth
Logical	Laeolus_column	ON to use the lidar column routine for AEOLUS
	Laeolus_subcolumn	ON to use lidar subcolumn routine for AEOLUS
	ok_lidar_cfad_aeolus	ON to compute lidar CFAD diagnostics
Outputs	aeolus_beta_tot	Total backscattered signal
	aeolus_beta_mol	Molecular backscatter
	aeolus_cfad_sr	CFAD of scattering ratio
	aeolus_lidarcld	3D cloud fraction
	aeolus_cldlayer	low, mid, high and total cloud cover
	aeolus_srbval	SR bins in cfad_sr

Table A1. Description of the new variables included in the Aeolus version of COSP-LIDAR

Appendix A: Additional technical details on the COSP-lidar/AEOLUS implementations

490 An "AEOLUS interface" has been implemented to define the AEOLUS-specific Fortran data type and to provide a dedicated, currently empty, initialization routine. The following table A1 provides the description of the new AEOLUS-specific variables added to the COSP algorithm.

The table A2 gives the list of the variables that are mandatory to run the COSP-lidar simulations in our developpement mode.

Variable name in COSP	Variable name in IPSL-CM6	Variable name in CMIP6 database	Dimension	Description	Frequencies available
uLOSaeolus	uLOSaeolus	ua	3D	northward wind	CFday
vLOSaeolus	vLOSaeolus	va	3D	eastward wind	CFday
psfc	psol	ps	2D	surface pressure	CFday
pfull	pres	pfull	3D	air pressure (full levels)	CF3hr, CFday
phalf	paprs	phalf	3D	air pressure (mid-levels)	CF3hr, CFday
height	zfull	zfull	3D	altitude of full pressure levels	CF3hr
height_half	zhalf	zhalf	3D	altitude of half pressure levels	CF3hr
T_abs	temp	ta	3D	air temperature	CF3hr, CFday
qv	ovap	hus	3D	specific humidity	CF3hr, CFday
rh	rhum	hur	3D	relative humidity	CFday
tca	rneb	cl		cloud fraction	CFday
cca	rnebcon	clc		convective cloud fraction	CF3hr
mr_lsice	icc3dstra	clis		mass fraction of stratiform cloud ice	CF3hr
mr_ccliq	lcc3dcon	clwc		convective cloud liquid fraction	CF3hr
mr_ccice	icc3dcon	clic		mass fraction of convective cloud ice	CF3hr
fl_lsrain	pr_lsc_i	prlsprof	3D	large scale precip liquid	CF3hr
fl_lssnow	pr_lsc_i	prlsns	3D	large scale precip ice	CF3hr
fl_ccrain	pr_con_i	prcprof	3D	convective precip liquid	CF3hr
fl_ccsnow	pr_con_i	prsnc	3D	convective precip ice	CF3hr
skt	tsol	ts	2D	surface temperature	CF3hr
orography	phis	orog	2D	surface geopotential height	fx
landmask	contfracATMO	sftlf	2D	% land surface	fx
Reff	ref_liq, ref_ice	reffclis, reffclws	3D		CF3hr

Table A2. Description of the model variables that are mandatory as inputs of COSP simulations